IEEE Open Journal of the
Industrial Electronics Society

Received 23 July 2022; revised 18 August 2022; accepted 22 August 2022. Date of publication 29 August 2022;
date of current version 9 September 2022. The review of this paper was arranged by Associate Editor Haitham Abu-Rub.

Digital Object Identifier 10.1109/OJIES.2022.3202431

Distributed Hierarchical Control for Fast Frequency Restoration in VSG-Controlled Islanded Microgrids

KUO FENG AND CHUNHUA LIU (Senior Member, IEEE)

School of Energy and Environment, City University of Hong Kong, Hong Kong SAR, China

(CORRESPONDING AUTHOR: CHUNHUA LIU.)

This work was supported in part by Environment and Conservation Fund and Woo Wheelock Green Fund, Hong Kong SAR, China under ECF Project 56/2021, in part by the Innovation and Technology Commission, Hong Kong SAR, China under Project ITS/045/21, in part by the City University of Hong Kong, Hong Kong SAR, China through an Applied Research under Grant 9667251, and in part by the Research Grants Council, Hong Kong SAR, China through Collaborative Research Fund under CRF Project C1052-21GF.

ABSTRACT As microgrids develop rapidly, more inverters are adopted to achieve DC/AC or AC/DC/AC conversion of distributed generators (DGs). The virtual synchronous generator (VSG) control has started to replace the traditional droop control for inverters. In order to restore the frequency to its nominal value, most existing secondary frequency control (SFC) methods are based on frequency measurements. However, while reducing the rate of change of frequency (ROCOF), virtual inertia also slows down the convergence of frequency-based SFC. Therefore, this paper proposes a new distributed hierarchical control for fast frequency restoration. Based on the real-time VSG control at the bottom level, a novel frequency restoration control is designed. The power reference values generated by the proposed control can accelerate the frequency restoration with accurate power sharing. Meanwhile, by designing event-triggering conditions, parallel inverter controllers only need to communicate with neighbors at the event-triggered moments. Simulations have been performed in MATLAB/Simulink environment. Furthermore, the proposed control has also been tested on the experiment platform, which contains practical physical circuits and real-time controllers. Both simulation and experiment results verify the effectiveness of the proposed control strategy.

INDEX TERMS Hierarchical control, islanded microgrid, parallel voltage source inverters (VSIs), real-time experiment, virtual synchronous generator (VSG).

I. INTRODUCTION

Microgrids [1] have been proven to achieve advantages for integrating DGs, EVs, and ESSs into power systems. In the microgrid, the operation of renewable energy generation and vehicle-to-grid (V2G) [2] generally is supported by inverters. However, inverters, as electronic devices, have no inertia themselves. The large-scale integration of inverters with microgrids has created significant challenges. The low inertia significantly affects the stability and dynamic performance of the power grid. Although the development of microgrids can insulate the random and intermittent renewable energy generation and V2G connection from the giant power grid, the stable and economic operation of the microgrid itself is still a challenge for researchers.

According to the control timescale, the microgrid control has hierarchical characteristics [1], including real-time primary control, secondary frequency control (SFC) and voltage control (SVC) [3], and tertiary economic dispatch control [4]. In the primary control, the droop control was first used for conventional generators, e.g., synchronous and induction generators [5]. As DC-AC inverter-feeding power systems became numerous, droop control was introduced for inverters [6], [7], [8]. Zhong's work [9] highlighted some drawbacks of the droop controller for inverters, especially compared to conventional generators. Some researchers have studied control methods that can provide virtual inertia for power grids during the last decade, called virtual synchronous generators (VSG) [10], [11], [12]. Reference [13] compared the droop control

and VSG control. It proved that the active power control loops for droop and VSG control are identical when some conditions are satisfied. Some other research works tried to improve the dynamic performance of VSG control with various control techniques [14], [15]. The VSG control belongs to the primary control, which has the steady-state error. So, secondary control is needed to restore the frequency and voltage to the nominal values.

Secondary control can be classified into three main categories: centralized, distributed, and decentralized secondary control [3]. For a centralized scheme [16], a control center is needed to collect and manage the global information, which may cause challenges to communication, computation, and privacy issues. Moreover, it is difficult for microgrid participants to achieve global frequency consensus only using local information. References [17] and [18] propose decentralized frequency control by adding active power estimation and small-ac-signal injection. With the development of communication technology and the reduction of communication costs, the distributed frequency control method has become more popular. Distributed control [19], [20] only utilizes neighboring information exchange and can achieve global consensus efficiently and reliably. In order to reduce the number of communication among neighbors, event-triggered distributed control was proposed. In [21], a distributed robust frequency restoration with an event-triggered strategy was proposed based on the primary droop control.

Based on the literature survey mentioned above, some exciting topics still need to be studied. First, the buffer time of frequency change in VSG control offers an opportunity for SFC to have better dynamic performance. Especially, most existing SFC is based on droop control [22], [23], while the virtual inertia supplied by VSG control is not considered. Second, the theoretical distributed algorithms usually need continual iterations. Frequent updating and broadcasting of the control inputs result in high cost and low practicality. Third, hardware in the loop (HiL) can test the operation of controllers [24] and electrical components [25] on the real-time grid simulation model. The construction of the actual physical circuit allows researchers to observe unforeseen disturbances in the electric circuit and their impact on the control. Experiments on it can better demonstrate the practicability and robustness of the proposed control algorithm.

Therefore, this paper proposes a distributed hierarchical control for parallel inverters with VSG regulation in an islanded microgrid. The main contributions are summarized as follows.

1) Based on the VSG primary control, the virtual inertia reduces the rate of change of frequency (ROCOF). However, the virtual inertia will also slow down the convergence rate of existing frequency-based SFC output at the same time. Therefore, a novel frequency restoration control is proposed in this paper. The generated power reference values can restore the frequency faster with less frequency variation when load disturbances happen.
2) An event-triggered strategy with trigger condition design is proposed. With the intermittent communication scheme, the communication burden for data exchange between DGs is highly reduced. The stability of the proposed distributed event-triggered frequency restoration control is also ensured. The proposed control scheme improves the feasibility of distributed algorithms in practical applications.

The proposed frequency restoration control is verified in both simulation and experiments. The experiment platform contains actual physical circuits and real-time control signals from MicroLabBox. The simulation and experiment results validate the effectiveness of the proposed control.

The paper is organized as follows. In Section II, the cyber-physical microgrid system is introduced. The proposed distributed event-triggered frequency restoration control is presented in Section III. Section III also proves the stability and discusses the lower bound of the interevent interval. Simulation and experimental verification are provided in Sections IV and V, respectively. Finally, the conclusion is stated in Section VI.

II. MODELING OF MICROGRID FREQUENCY CONTROL

In this work, a distributed event-triggered frequency restoration control is proposed for a cyber-physical microgrid system. The physical system contains the electrical circuit and local controllers for inverters. With the PWM signals generated by the real-time simulator, the practical electrical circuit will operate to simulate the primary frequency control response of an islanded microgrid. The cyber system is to realize the communication among agents. Through multiple iterations of calculation and communication, the distributed event-triggered frequency restoration algorithm can give accurate power reference values and restore the frequency to its rated value.

A. PHYSICAL SYSTEM

1) ELECTRICAL CONNECTION

The microgrid adopted in this paper is islanded and supplied by DGs with renewable energy sources, energy storage devices, or EVs. These DGs are integrated into the microgrid via voltage source inverters (VSIs). Parallel VSIs operate in grid-forming mode. The digital control signals for the inverters aim to coordinate the output voltage and frequency. Meanwhile, the output power should follow the power sharing proportion accurately. The structure of the microgrid can be found in Fig. 1. When batteries act as DC sources, half-bridge inverters are needed to generate AC. After the LC filter, batteries connect to the other sources in parallel. Through the point of common coupling (PCC), power is transmitted directly to the common load.

2) PRIMARY VSG CONTROL

In order to imitate the droop characteristic of traditional generators, local droop control is adopted to control the frequency

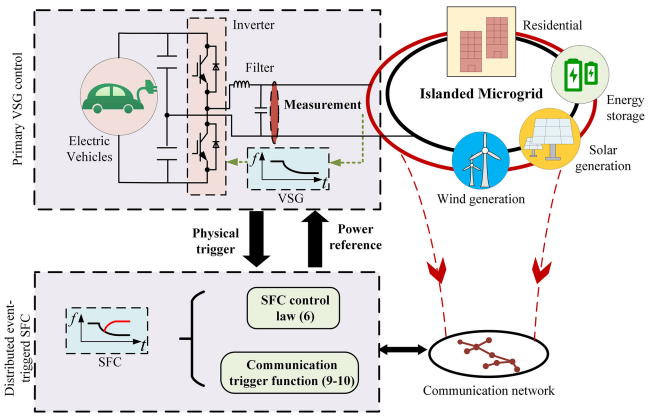

FIGURE 1. Diagram of an islanded microgrid with primary and secondary frequency control.

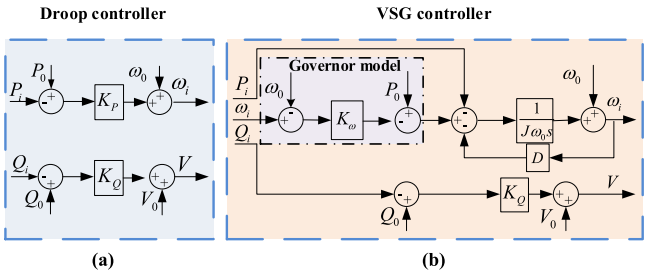

FIGURE 2. Control loop of droop control and VSG control. (a) Droop control. (b) VSG control.

and voltage of inverters. However, the droop control for inverters can provide little inertia for microgrids. An inertia-lacking power grid will be sensitive to faults, and its steady and dynamic performance will be significantly impacted. In order to provide inertia support for the power grid, the VSG control is proposed to mimic the transient characteristics of a synchronous generator by emulating its fundamental swing equation. Considering the mechanical model and frequency governor of the synchronous generator, the local primary VSG control can be modeled as:

$$J\omega_0 \frac{d\omega}{dt} = P_{\text{in}} - P - D(\omega - \omega_0), \tag{1}$$

$$P_{in} = P_0 - K_\omega(\omega - \omega_0), \tag{2}$$

where ω_0 and ω are the nominal and measured frequency respectively; P, P_0, and P_{in} are the measured output, reference value and governor reference value of active power respectively; J and D represent the moment of inertia and the damping factor. (2) is the governor model. K_ω is the proportional coefficient. The control loop of VSG is shown in Fig. 2(b). It can replace the droop control loop in Fig. 2(a).

The proportional coefficient K_ω in the governor model and the damping factor D both can change the steady state after primary control. The larger the inertia J is, the more gently frequency will decrease. The parameters $1/K_P$ or $(K_\omega + D)$ with the difference of frequency decide the steady state. Moreover, virtual inertia J only influences the transient response.

Based on equations (1) and (2), the primary VSG control for a node i can be rewritten as (3) and (4),

$$\dot{\theta}_i = \omega_i, \tag{3}$$

$$M_i\dot{\omega}_i + D_i(\omega_i - \omega_0) = P_{0i} - P_i - u_i, \tag{4}$$

where $D_i = K_{\omega i} + D_i$, $M_i = J_i\omega_0$, θ_i is the nodal voltage phase angle, and u_i is the SFC compensatory output. $P_{0i} - u_i$ is the active power reference generated by the SFC, which is considered to be constant in the primary VSG control. For inductive lines of susceptance B_{ij} connecting bus i to bus j, the active power is given by $P_i = \sum_j |B_{ij}|V_iV_j \sin(\theta_{ij})$.

Instead of the primary droop control, the proposed SFC is based on the VSG control. The transfer function of frequency and output power can be deduced from (4) and Fig. 2(b). The transfer function and the time constant T_i are illustrated as follows.

$$\frac{\Delta\omega_i}{\Delta P_i} = \frac{-1}{M_is + D_i} = \frac{K_i}{T_is + 1}, \text{ where } T_i = \frac{M_i}{D_i}, K_i = -\frac{1}{D_i} \tag{5}$$

The settling time is defined as the minimum time required for the response curve to reach and no longer exceed the $\pm 5\%$ error band. Therefore, the settling time of the VSG control is $t_s = 3T_i$. It means that, after the load change, the frequency under the VSG control needs $3T_i$ to achieve the steady state.

B. CYBER SYSTEM

1) COMMUNICATION NETWORK

When considering a microgrid with communication infrastructure, the microgrid can be modeled by the algebraic graph theory. Nodes in the microgrid can be indexed by $i \in N$, $N := \{1, \ldots, n\}$. The DG nodes in set N are indexed by $i \in G$, $G := \{1, \ldots, \text{n} - 1\}$. The total number of DG nodes is $g = n - 1$.The load node in set N is indexed by $i = n$. Assumed that communication links only exist among DGs, DGs can be abstracted as a graph $DG := (G, E, A)$. The communication link which connects DG node i and DG node j is denoted as $(i, j) \in E$. A is the $g \times g$ weighted adjacency matrix. In A , if node i communicates with node j, $a_{ij} = a_{ji} > 0$. Γ is the corresponding Laplacian matrix. The in-degree matrix is defined as $D_d = \text{diag}(d_i)$, where $\text{d}_i = \sum_j^G a_{ij}$. Let $\mathbf{1}_n$ and $\mathbf{0}_n$ be the n-dimensional vectors of all ones and all zeros.

2) EVENT-TRIGGERED MECHANISM

The proposed SFC scheme has two timescales. One is the broadcast rate of power references generated by the SFC. The slow broadcast rate will avoid the fluctuation caused by frequent changes in power reference values. Meanwhile, the slow broadcast rate contributes to exhibiting the SFC control performance. The other one is the communication trigger. It is designed to reduce the communication burdens in one SFC interval. The agents do not need to communicate with neighbors in all calculation iterations. A 1-ms interval is adopted to denote the minimal communication period of the existing

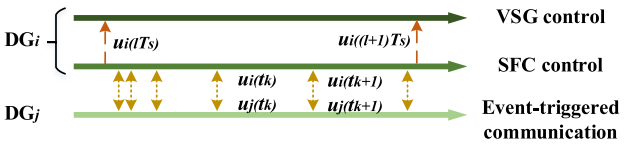

FIGURE 3. Control moments in the proposed control structure.

communication network by reference to 5G technology. The corresponding diagram is shown in Fig. 3.

III. PROPOSED DISTRIBUTED EVENT-TRIGGERED FREQUENCY RESTORATION CONTROL

A. PROPOSED CONTROLLER

The control moments diagram of the proposed distributed hierarchical frequency restoration control is shown in Fig. 3. The primary VSG control at the bottom level is applied to inverters as (3) and (4) in real-time operation. The reference generated by SFC at the second level will be broadcasted at T_s rate. Within one T_s, the SFC controller will communicate with neighbors at the event-triggered time to update the control input u. Thus, the communication burdens will be reduced.

The frequency restoration controller based on the primary VSG control is proposed as follows.

$$\dot{u}_i(t) = P_{0i} - P_i - u_i(t) - k \sum_{j\in G, ij\in E} a_{ij}\left(\frac{u_i(t_h)}{D_i} - \frac{u_j(t_h)}{D_j}\right). \tag{6}$$

In (6), k is a positive gain. When the weighted adjacency matrix A with elements a_{ij} satisfies $A \neq 0$, in the steady state, $\omega_i - \omega_0 = 0$ and $u_i/D_i = u_j/D_j$ are achieved simultaneously. It means that the secondary control output u_i will compensate for the load changes. The frequency will be restored to its nominal value ω_0. Meanwhile, the active power sharing will be realized proportionally.

Note that the communication section

$$k \sum_{j\in G, ij\in E} a_{ij}\left(\frac{u_i(t_h)}{D_i} - \frac{u_j(t_h)}{D_j}\right) \tag{7}$$

in (6) is updated only at the event-triggered moments rather than the fixed periodical time interval.

The state measurement error is calculated from

$$e_i(t) = u_i(t_h) - u_i(t),\ t \in [t_h, t_{h+1}) \tag{8}$$

The control law proposed in (6) ensures the power sharing and frequency restoration of the islanded microgrid with parallel inverters if the event-triggered time is defined as:

$$t_h = \inf\{t > t_{h-1} | f_i(t) = 0\} \tag{9}$$

where the trigger function $f_i(t)$ of agent i can be defined as

$$f_i(t) = \left\|\frac{e_i}{D_i}\right\|^2 - \beta\frac{\alpha(\lambda_{\min} - \alpha k d_i)}{k d_i}\left\|\frac{u_i}{D_i}\right\|^2 \tag{10}$$

The coefficient $0 < \beta < 1$. Furthermore, there is

$$0 < \alpha < \frac{\lambda_{min}}{k d_i},\ \forall i, \tag{11}$$

where λ_{min} is the minimum eigenvalue of $k\Gamma + \frac{1}{2}D_G$. Considering the properties of Laplacian matrix Γ , $\lambda_{min} > 0$.

B. STABILITY ANALYSIS

To achieve the synchronization of the whole microgrid, the load in the microgrid is modeled as a bulk frequency responsive load, which is not controllable but related to the primary frequency control. Therefore, its model is shown as:

$$\dot{\theta}_L = \omega_L \tag{12a}$$

$$P_L = P_{0L} - D_L(\omega_L - \omega_0) \tag{12b}$$

where P_L is the load supplied. The uncontrollable load is assumed to consist of a constant load P_{0L} and a frequency-dependent component with $0 \le D_L \le D_{tot}$, where $D_{tot} = \sum_{i\in G} D_i$, [26]. In addition, power supplies are positive values, whereas loads are negative values in the calculation.

Note: The load model in (12) helps to model the islanded microgrid. Meanwhile, there is no controller on the load side. The power references $P_{0i} - u_i$ in (4) of DGs are the secondary control outputs that need to be solved.

For convenient representation, matrices are introduced as

$$D = diag(D_G, D_L),\ M = diag(M_i) \in \mathbb{R}^{g\times g}.$$

Moreover, vectors are introduced as

$$P_{0G} = col(P_{oi}) \in \mathbb{R}^g,\ \ u = col(u_i) \in \mathbb{R}^g,\ \ e = col(e_i) \in \mathbb{R}^g.$$

Also, the potential function $U : \mathbb{R}^n \to \mathbb{R}$ is introduced, see [26],

$$U(\theta) = -\sum_{i\in G, j=n} |B_{ij}| V_i V_j \cos(\theta_{ij}). \tag{13}$$

$U(\theta)$ is a convex function when $\theta_{ij} \in \left[-\frac{\pi}{2}, \frac{\pi}{2}\right]$. Due to the power flow in the microgrid, the following equation can be obtained.

$$\mathbf{1}_n^T \nabla_\theta U(\theta) = \sum_{i=1}^{g} P_i + P_L = 0. \tag{14}$$

Then the overall frequency restoration model with event-triggered communication is shown as follows,

$$\dot{\theta}_G = \omega_G, \tag{15a}$$

$$M\dot{\omega}_G = -D_G(\omega_G - \omega_0\mathbf{1}_n) + P_{0G} - \nabla_{\theta G}U(\theta) - u, \tag{15b}$$

$$D_L\dot{\theta}_L = D_L\omega_0 + P_{0L} - \nabla_{\theta L}U(\theta), \tag{15c}$$

$$\dot{u} = P_{0G} - \nabla_{\theta G}U(\theta) - u - k\Gamma D_G^{-1}(u + e), \tag{15d}$$

where $\Gamma = \Gamma^T \in \mathbb{R}^{g\times g}$ is the Laplacian matrix of DGs in the islanded microgrid. Equations (15a-b) are the *P-f* characteristics of DGs with the VSG control and SFC input u. (15c) is the uncontrollable load model with the frequency-dependent component. Based on the state measurement error in (8), the

proposed control input with the event-triggered communication can be modeled in matrix form, as in (15d).

In steady state, $\dot{\theta} = \omega_0 \mathbf{1}_n$, $\dot{\omega} = \mathbf{0}_n$, and $\dot{u} = \mathbf{0}_n$. Therefore, from

$$\begin{bmatrix} P_{0G} - \nabla_{\theta G} U(\theta) - u \\ P_{0L} - \nabla_{\theta L} U(\theta) \end{bmatrix} = \mathbf{0}_n,$$

From (15d), $k\Gamma D_G^{-1}(u+e) = 0$, which means $u_i(t_k)/D_i = u_j(t_k)/D_j$. This ensures proportional power sharing.

With the solution $\mathrm{col}(\theta^*, \omega^*, \mathrm{u}^*) \in \mathbb{R}^n \times \mathbb{R}^g \times \mathbb{R}^g$ in proposition 1, the error states are introduced as

$$\tilde{\omega}(t) = \dot{\theta}(t) - \omega^* 1_n = \omega(t) - \omega^* 1_n \in \mathbb{R}^n,$$
$$\tilde{\theta}(t) = \theta(0) + \int_0^t \tilde{\omega}(\tau) d\tau \in \mathbb{R}^n,\ \tilde{u}(t) = u(t) - u^* \in \mathbb{R}^g.$$
$$\nabla_{\tilde{\theta} G} U(\tilde{\theta}_G) = \nabla_{\tilde{\theta}^* G} U(\tilde{\theta}_G^*) + D_G \mathbf{1}_g \tfrac{D_L \tilde{\omega}_L}{D_{tot}}$$

$\nabla_{\tilde{\theta} G} U(\tilde{\theta}_G^*)$ is the power supply $\nabla_{\tilde{\theta} G} U(\tilde{\theta}_G)$ at ω^*. In order to satisfy the frequency-dependent component in load, the power supply error is also frequency-dependent.

Then, equations in (15) become

$$\dot{\tilde{\theta}}_G = \tilde{\omega}_G, \tag{16a}$$

$$M\dot{\tilde{\omega}}_G = -D_G \tilde{\omega}_G + \nabla_{\tilde{\theta}^* G} U\left(\tilde{\theta}^*\right) - \nabla_{\tilde{\theta} G} U\left(\tilde{\theta}\right) - \tilde{u}, \tag{16b}$$

$$D_L \dot{\tilde{\theta}}_L = \nabla_{\tilde{\theta}^* L} U\left(\tilde{\theta}^*\right) - \nabla_{\tilde{\theta} L} U\left(\tilde{\theta}\right), \tag{16c}$$

$$\dot{\tilde{u}} = \nabla_{\tilde{\theta}^* G} U\left(\tilde{\theta}^*\right) - \nabla_{\tilde{\theta} G} U\left(\tilde{\theta}\right) - \tilde{u} - k\Gamma D_G^{-1}(\tilde{u} + e). \tag{16d}$$

If and only if the equilibrium solution $\mathrm{col}(\theta^*, \omega^*, \mathrm{u}^*) \in \mathbb{R}^n \times \mathbb{R}^g \times \mathbb{R}^g$ in proposition 1 existed, then the system (15) owns a unique equilibrium solution $\mathrm{col}(\tilde{\theta}^*, \tilde{\omega}^*, \tilde{\mathrm{u}}^*) = \mathrm{col}(\tilde{\theta}^*, \mathbf{0}_n, \mathbf{0}_n)$.

Likewise, the asymptotic stability of (16) with its equilibrium $\mathrm{col}(\tilde{\theta}^*, \tilde{\omega}^*, \tilde{\mathrm{u}}^*)$ implies asymptotic convergence of system (15) with its equilibrium solution $\mathrm{col}(\theta^*, \omega^*, \mathrm{u}^*)$. So, the following content will prove the local asymptotic stability of (16).

Before proving the local asymptotic stability, refer to the uniqueness and existence theorem in [27], the ordinary differential equations (ODEs) (16a–d) are continuous and satisfy the Lipschitz condition with an initial value $\mathrm{col}(\tilde{\theta}_0, \tilde{\omega}_0, \tilde{u}_0)$. Then system (15) has a unique solution $\mathrm{col}(\theta^*, \omega^*, \mathrm{u}^*)$.

Our main result of this section is as follows.

Proposition 1 (Stability of equilibrium): Consider the system (16), then the equilibrium point $\mathrm{col}(\tilde{\theta}^*, \tilde{\omega}^*, \tilde{\mathrm{u}}^*) = \mathrm{col}(\tilde{\theta}^*, \mathbf{0}_n, \mathbf{0}_n)$ with $\tilde{\theta}^* \in \Theta$ is locally asymptotic stable. □

Proof: Inspired by [28], a Lyapunov candidate function is constructed as

$$V\left(\tilde{\theta}, \tilde{\omega}_G, \tilde{u}\right) = \frac{1}{2}\tilde{\omega}_G^T M \tilde{\omega}_G + U\left(\tilde{\theta}\right) - U\left(\tilde{\theta}^*\right) - \nabla_{\tilde{\theta}^*} U\left(\tilde{\theta}^*\right)^T \left(\tilde{\theta} - \tilde{\theta}^*\right) + \frac{1}{2}\tilde{u}^T D_G^{-1} \tilde{u} \tag{17}$$

The Bregman distance of $U(\theta)$ to $\tilde{\theta}^*$ is used. The following partial derivatives can be got.

$$\nabla V|_{z^*} = col\left(\nabla_{\tilde{\theta}} U\left(\tilde{\theta}\right) - \nabla_{\tilde{\theta}^*} U\left(\tilde{\theta}^*\right), M\tilde{\omega}_G, D_G^{-1}\tilde{u}\right)|_{z^*} = \mathbf{0}_{(n+2g)}$$

$$\nabla^2 V|_{z^*} = blkdiag\left(\tilde{L}_e, M, D_G^{-1}\right)|_{z^*} \in \mathbb{R}^{(n+2g)\times(n+2g)}$$

where $\tilde{L}_e \in \mathbb{R}^{n\times n}$ is the Laplacian matrix with elements.

$$\tilde{L}_e = \frac{\partial^2 U(\tilde{\theta})}{\partial \tilde{\theta}_j \partial \tilde{\theta}_i} = \begin{cases} -\left|B_{ij}\right| V_i V_j \cos\left(\tilde{\theta}_{ij}\right) & if\ j \neq i, \\ \sum_{k=1, k\neq i}^{N} |B_{ik}| V_i V_k \cos\left(\tilde{\theta}_{ik}\right) & if\ j = i. \end{cases}$$

Considering the characteristics of the Laplacian matrix, $\tilde{L}_e$ is positive semidefinite and irreducible. M, D_G^{-1} are also positive definite. Consequently, z^* is a strict minimum point of V. Moreover, V is locally positive definite around the equilibrium point z^*.

Then, the derivative of V along trajectories (16) is

$$\dot{V} = \tilde{\omega}_G^T M \dot{\tilde{\omega}}_G + \left(\nabla U\left(\tilde{\theta}\right) - \nabla U\left(\tilde{\theta}^*\right)\right)^T \dot{\tilde{\theta}} + \tilde{u}^T D_G^{-1} \dot{\tilde{u}}. \tag{18}$$

Lemma 1 [29]: For any $a,\ b \in \mathbb{R}^n$ and any symmetric positive-definite matrix $\Phi \in \mathbb{R}^{n\times n}$, $2|a^T b| \leq a^T \Phi^{-1} a + b^T \Phi b$.

Lemma 2 [29]: **(Rayleigh-Ritz theorem)** Let $A \in \mathbb{R}^{n\times n}$ be symmetric. Then $\lambda_{min}(A) x^T x \leq x^T A x$.

The detailed calculation process is shown as follows.

$$\begin{aligned} \dot{V} =& -\tilde{\omega}_G^T D_G \tilde{\omega}_G - \tilde{\omega}_G^T \tilde{u} - \tilde{\omega}_L^T D_L^{-1} \tilde{\omega}_L - \tilde{u}^T D_G^{-1} k\Gamma D_G^{-1}(\tilde{u}+e) \\ &+ \tilde{u}^T D_G^{-1}\left(\nabla_{\tilde{\theta}^* G} U\left(\tilde{\theta}^*\right) - \nabla_{\tilde{\theta} G} U\left(\tilde{\theta}\right)\right) - \tilde{u}^T D_G^{-1} \tilde{u} \\ \leq& -\tilde{\omega}_L D_L \tilde{\omega}_L - \tilde{u}^T \mathbf{1}_g \frac{D_L \tilde{\omega}_L}{D_{tot}} \\ &-\frac{3}{4}\tilde{u}^T D_G^{-1} \tilde{u} - \tilde{u}^T D_G^{-1} k\Gamma D_G^{-1}(\tilde{u}+e) \\ \leq& -\frac{1}{2}\tilde{u}^T D_G^{-1} \tilde{u} - \tilde{u}^T D_G^{-1} k\Gamma D_G^{-1}(\tilde{u}+e) \end{aligned}$$

Using Lemma 1, the scaling operations are achieved. The last remaining item is the event-triggered communication section. With Lemma 1 and Lemma 2,

$$\begin{aligned} \dot{V} \leq& -\frac{1}{2}\tilde{u}^T D_G^{-1} \tilde{u} - \tilde{u}^T D_G^{-1} k\Gamma D_G^{-1}(\tilde{u}+e) \\ \leq& -\lambda_{\min} \sum_{i=1}^{g} \left(\frac{u_i}{D_i}\right)^2 - \sum_{i=1}^{g} k d_i \frac{u_i}{D_i}\frac{e_i}{D_i} + \sum_{i=1}^{g}\sum_{j\in N_i} k \frac{u_i}{D_i}\frac{e_j}{D_j} \\ \leq& -\lambda_{\min} \sum_{i=1}^{g} \left(\frac{u_i}{D_i}\right)^2 + k\frac{\alpha}{2}\sum_{i=1}^{g} d_i \left(\frac{u_i}{D_i}\right)^2 + k\frac{1}{2\alpha}\sum_{i=1}^{g} d_i \left(\frac{e_i}{D_i}\right)^2 \\ &+ k\frac{\alpha}{2}\sum_{i=1}^{g}\sum_{j\in N_i}\left(\frac{u_i}{D_i}\right)^2 + k\frac{1}{2\alpha}\sum_{i=1}^{g}\sum_{j\in N_i}\left(\frac{e_j}{D_j}\right)^2 \end{aligned} \tag{19}$$

Considering that graph G is undirected,

$$\sum_{i=1}^{g}\sum_{j\in N_i}\left(\frac{e_j}{D_j}\right)^2 = \sum_{i=1}^{g}\sum_{j\in N_i}\left(\frac{e_i}{D_i}\right)^2 \text{ and } \sum_{j\in N_i} a_{ij} = d_i.$$

Placing the above equations in (19) yields,

$$\dot{V} \leq -\sum_{i=1}^{g}(\lambda_{\min} - k\alpha d_i)\left(\frac{u_i}{D_i}\right)^2 + k\frac{1}{\alpha}\sum_{i=1}^{g} d_i \left(\frac{e_i}{D_i}\right)^2$$

Considering the triggering function $f(t)$ and (11),

$$\dot{V} \leq \sum_{i=1}^{g} (\beta - 1)(\lambda_{\min} - \alpha k d_i) \left(\frac{u_i}{D_i}\right)^2 \leq 0$$

Then z^* is a stable equilibrium point. Furthermore, no solution other than $\Lambda = 0$ can achieve $\dot{V} = 0$. All the conditions of LaSalle's invariance principle, which can be found in [30], are met. z^* of the system (16) is locally asymptotic stable. ■

The asymptotic stability proof of equilibrium point z^* to the system (16) implies asymptotic convergence of system (15) with its equilibrium solution col$(\theta^*, \omega^*, \mathrm{u}^*)$. Therefore, the control output u^* will recover the frequency of the microgrid ω to its nominal value $\omega^* = \omega_0$ and ensure proportional power sharing. The secondary frequency control problem with VSG primary control is solved.

C. MINIMAL INTEREVENT INTERVAL

In order to verify that the Zeno behavior can be avoided, the lower bound of the interevent interval is calculated. When the increase rate of e/u is maximum, the trigger interval is the shortest. Considering (10), the derivative of e/u for $t \in [t_h, t_{h+1})$ is

$$\frac{d}{dt}\frac{\|e\|}{\|u\|} = \frac{d}{dt}\frac{\left(e^T e\right)^{1/2}}{\left(u^T u\right)^{1/2}} \leq \left(1 + \frac{\|e\|}{\|u\|}\right)\frac{\|\dot{u}\|}{\|u\|} \tag{20}$$

From (15d) of $\dot{u}$,

$$\frac{d}{dt}\frac{\|e\|}{\|u\|} \leq l\left(1 + \frac{\|e\|}{\|u\|}\right)^2 = \Phi(t, \Phi_0), \tag{21}$$

where l is the Lipschitz constant for $\|\dot{u}\| \leq l\|u\| + l\|e\|$[31]. Thus, e/u is upper bounded by $\Phi(t, \Phi_0)$ which is the solution of

$$\begin{cases} \dot{\Phi} = l \cdot (1 + \Phi)^2 \\ \Phi(0, \Phi_0) = \Phi_0 \end{cases} \tag{22}$$

And $\Phi(\tau, 0) = \frac{\tau l}{1 - \tau l}$. Thus, the minimum interevent interval is obtained:

$$\tau_{\min} = \frac{\sqrt{\beta \frac{\alpha(\lambda_{\min} - \alpha k d_i)}{d_i}}}{\left(1 + \sqrt{\beta \frac{\alpha(\lambda_{\min} - \alpha k d_i)}{k d_i}}\right) l} \tag{23}$$

τ_{min} proves that the proposed system avoids the Zeno behavior.

IV. SIMULATION VERIFICATION

To verify the effectiveness of the proposed frequency restoration control, an islanded microgrid with three parallel DGs is used, as shown in Fig. 4. The virtual impedance and V-I dual-loop PR conptrol are adopted to generate the voltage signal for the parallel inverters. The voltage after the LC filter will track the voltage reference accurately. Simulation parameters are listed in Table 1. Due to the decoupling of frequency control and voltage control, the frequency of the microgrid is only influenced by the active power consumption. The pure inductive load only consumes the reactive power. When the RL load is connected to the microgrid, the control performance of our proposed SFC is still effective. The communication among these three DGs has a Laplacian matrix Γ, which is used in (15d) and (16d).

$$\Gamma = \begin{pmatrix} 1 & -1 & 0 \\ -1 & 2 & -1 \\ 0 & -1 & 1 \end{pmatrix}$$

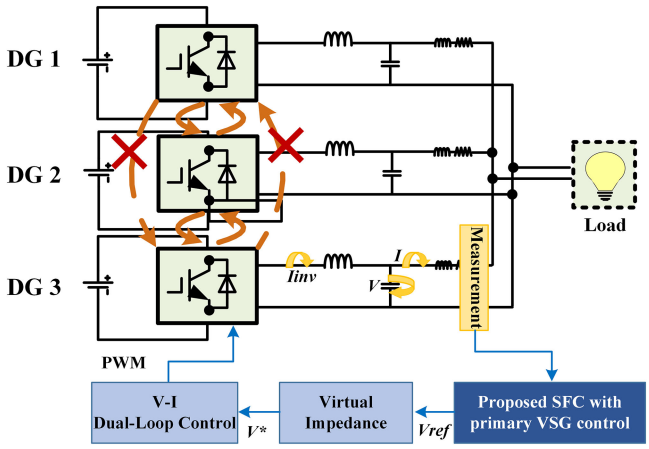

FIGURE 4. Islanded microgrid with three parallel DGs.

TABLE 1 Simulation Parameters of Studied Islanded Microgrid

Symbol	Description	Value		
V_{DC}	DC voltage supply (V)	700		
V	Rated AC voltage (V_{peak})	311		
ω_0	Rated angular frequency (rad/s)	$2\pi \times 50$		
f_{sa}	Sampling frequency (kHz)	20		
f_{sw}	Switching frequency (kHz)	10		
P_L	load 1 and 2 (kW)	2, 1		
		DG 1	DG 2	DG 3
L_f	Filter inductance (mH)	15		
C_f	Filter Capacitance (μF)	45		
J_i	Virtual inertia (kg · m^2)	2	1	2/3
D_i	VSG damping coefficient (W/rad/s)	120π	60π	40π
K_Q	$Q - V$ droop coefficient (V/var)	0.01	0.02	0.03
ω_c	Cutoff angular frequency of LPF (rad/s)	200	200	200
$k_{pv} + k_{iv}$	Voltage PR regulator	2+5		
$k_{pi} + k_{ii}$	Current PR regulator	1+1		
L_v	Virtual impedance (mH)	12	24	36
Z_i	Line impedance (Ω)	0.1+ j0.06	0.05+ j0.03	0.2+ j0.06

A. SIMULATION RESULTS OF DROOP AND VSG PRIMARY CONTROL

Fig. 5 shows the simulation results of droop and VSG primary control with load transitions. At 10 s, load 2 is connected. Then load 2 is disconnected after 50 s. The virtual inertia provided by the VSG control can reduce the ROCOF, while the

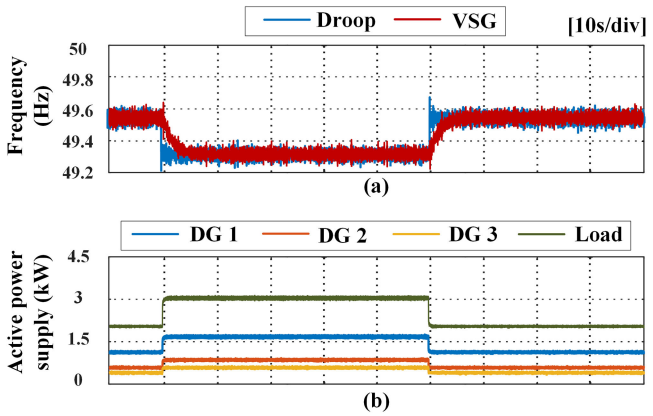

FIGURE 5. Control result of primary droop and VSG control. (a) Frequency of primary droop and VSG control. (b) Active power supply of three DGs and the total load at PCC.

steady-state deviations are the same as droop control. Meanwhile, three DGs share the active power supply proportionally and automatically. Results of the droop and VSG control verify the accuracy of primary control and the feasibility of islanded microgrid built in Simulink.

B. COMPARISON OF FREQUENCY-BASED SFC AND PROPOSED SFC

The control inputs in [28], [32], [33] are based on frequency measurements. A classical frequency-based SFC shown in (24) is chosen as a comparison.

$$k_i \dot{u}_i = -(\omega_i - \omega_0) - \sum_{j \in N, ij \in E} a_{ij} \left(\frac{u_i}{D_i} - \frac{u_j}{D_j} \right). \tag{24}$$

Based on the same primary VSG control parameters and operation environment, the comparison results with $T_s = 0.5s$ are shown in Fig. 6. The classical frequency-based SFC needs multiple updates to restore the frequency, which is slower than the proposed SFC. After the load disturbance, the following control input generated by the proposed SFC can provide nearly accurate power references. Due to the virtual inertia of VSG control, the frequency deviation is smaller. The frequency dynamic performance is more stable. Moreover, from Fig. 6(c), the power sharing keeps proportional. The frequency curves in the red rectangular are zoomed in and shown in Fig. 6(d). When a step change of active power load happens, the proposed SFC can quickly control the frequency back to the rated value. Fig. 6(e) and (f) are the results when the loss of communication between DG2 and DG3 disconnects the graph. The active power references of DGs cannot maintain an accurate power-sharing proportion. The disproportional references influence the power supply of DGs and make the operation of the islanded microgrid unstable.

In order to see the influence of T_s on different control methods, the simulation results of three control methods with $T_s = 2s$ are shown in Fig. 7. From the comparison, it can be

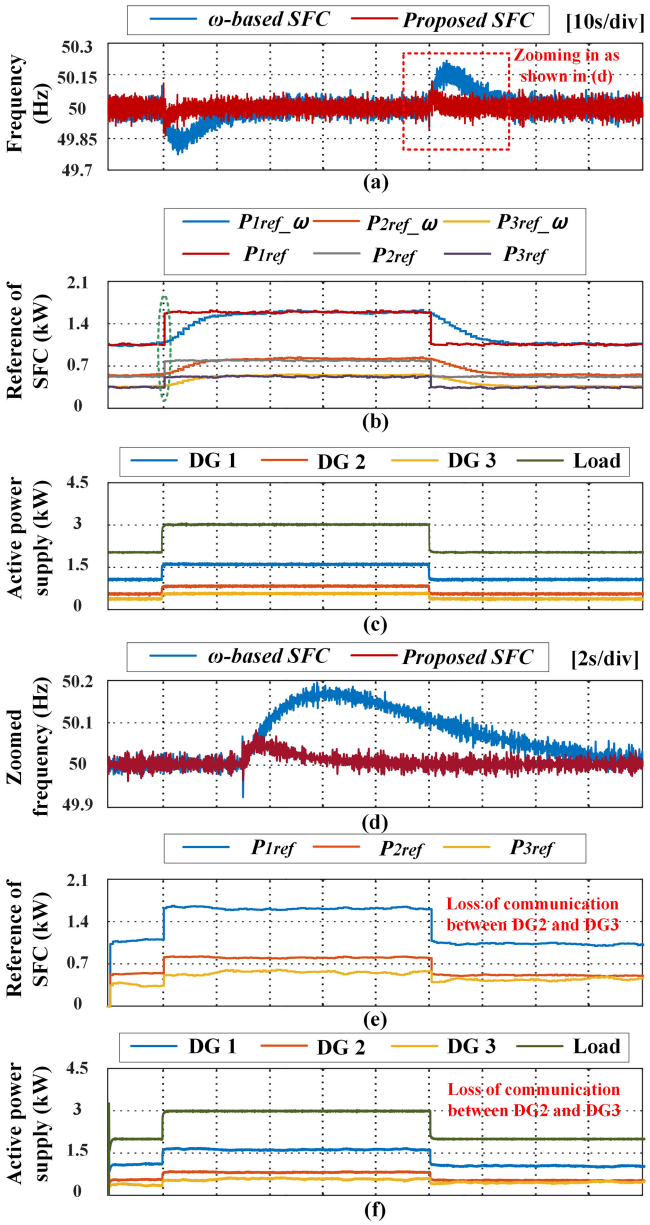

FIGURE 6. Comparison of frequency-based SFC and proposed SFC. (a) Frequency at PCC. (b) Active power references of three DGs broadcasted at $T_s = 0.5s$. (c) Active power supply of three DGs and the total load at PCC. (d) Zoomed frequency curve. (e) Active power reference with the loss of communication. (f) Active power supply and load with the loss of communication.

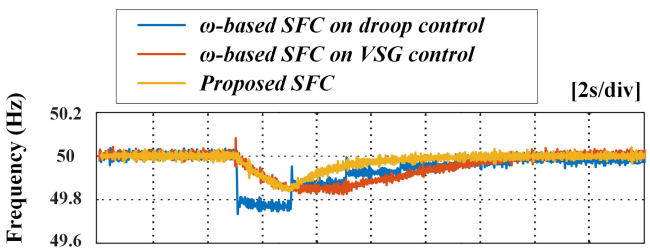

FIGURE 7. Comparison of different SFC control methods.

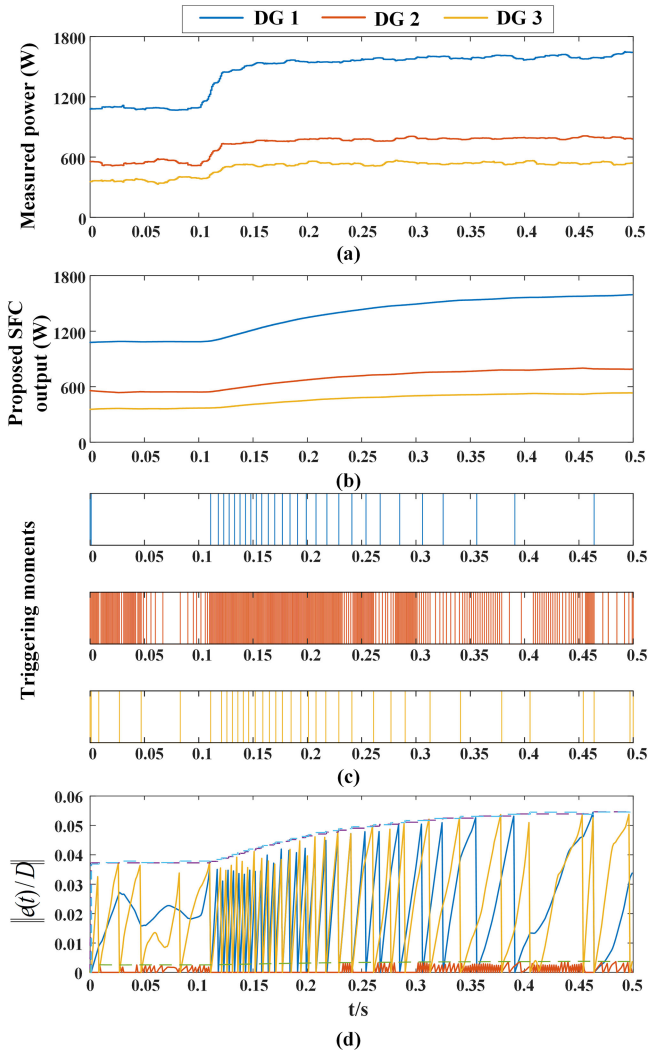

FIGURE 8. Proposed SFC iterations in 0.5s. (a) Measured active power of three DGs. (b) Iterations of control u. (c) Communication moments. (d) Estimate errors.

seen that the droop control will lead to a high ROCOF. The virtual inertia provided by the VSG control can decrease the ROCOF visibly. The convergence of ω-based SFC is slower than the proposed SFC.

C. PERFORMANCE OF THE EVENT-TRIGGERED COMMUNICATION

In order to show the effectiveness of event-triggered communication, the 0.5s time slot circled by the green oval in Fig. 6(b) is chosen. The specific operation of the control input updating and communication triggering moments is shown in Fig. 8. Considering the existing communication technology, a 1-ms interval is adopted to denote the minimal communication period [34]. Fig. 8(a) shows the active power of three DGs, which can be measured locally. The power references in Fig. 8(b) are updated by the control method in (15d). When the triggering function in (10) is triggered, DGs communicate with neighbors to adjust output. Table 2 lists the communication trigger times and the final broadcast power references. If traditional continuous communication is adopted, 1500 times of communication are needed for three DGs. With the proposed event-triggered SFC, more than 75% of communication is saved.

TABLE 2 Performance of Proposed SFC Iteration in 0.5s

	DG 1	DG 2	DG 3
Communication triggers	25	300	33
Broadcast control output at 0.5s (W)	1611	797	539

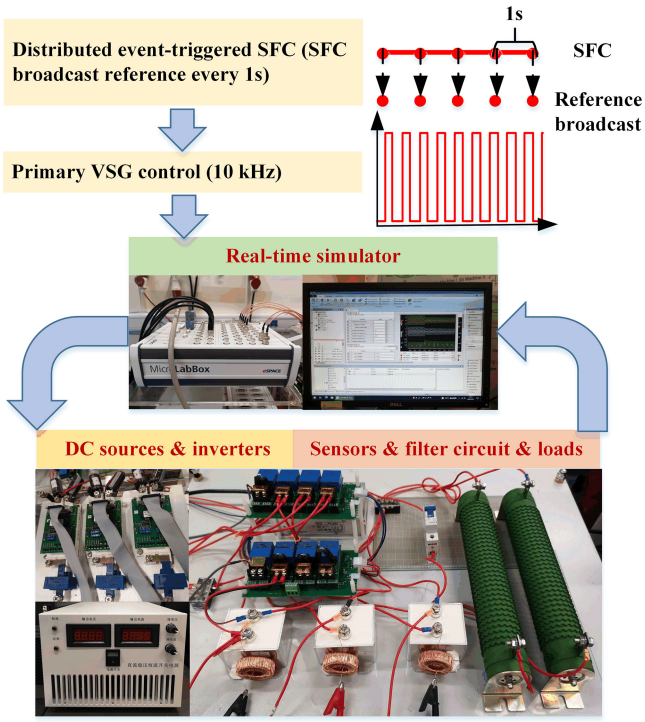

FIGURE 9. Experimental platform photograph.

V. EXPERIMENTAL VERIFICATION

In order to further verify the effectiveness of the proposed VSG-based SFC method, an experimental platform is established, as shown in Fig. 9. The primary VSG control and proposed SFC actions are given by the real-time simulator, MicroLabBox. Three DC sources with single-phase inverters, Infineon FF300R12ME4, are used to supply AC voltage. The voltage and current measurements are taken with Hall-effect sensors. Through LC filters, three DGs are paralleled to supply resistive loads. The physical circuit and communication paths are the same with simulation as shown in Fig. 4.

The parameters of the microgrid circuit and the control system are listed in Table 3. In order to verify the effectiveness of the microgrid experiment testbed, the primary VSG control is applied to three parallel inverters on the testbed.

TABLE 3 Experiment Parameters of Studied Islanded Microgrid

Symbol	Description	Value		
V_{DC}	DC voltage supply (V)	120		
V	Rated AC voltage (V)	50		
ω_0	Rated angular frequency (rad/s)	$2\pi \times 50$		
f_{sa}	Sampling frequency (kHz)	10		
f_{sw}	Switching frequency (kHz)	2		
R_L	Resistive load (Ω)	20, 20		
		DG 1	DG 2	DG 3
L_f	Filter inductance (mH)	15		
C_f	Filter Capacitance (μF)	45		
J_i	Virtual inertia ($kg \cdot m^2$)	0.15	0.075	0.05
$K_{\omega i}$	Proportional coefficient in the governor model (W/rad/s)	1/4	1/8	1/12
D_i	VSG damping coefficient (W/rad/s)	12π	6π	4π
K_Q	$Q-V$ droop coefficient (V/var)	0.005	0.01	0.015
$k_{pv}+k_{iv}$	Voltage regulator	0.36+0.01		
$k_{pi}+k_{ii}$	Current regulator	4.22+0.5		
L_v	Virtual impedance (mH)	3	6	9

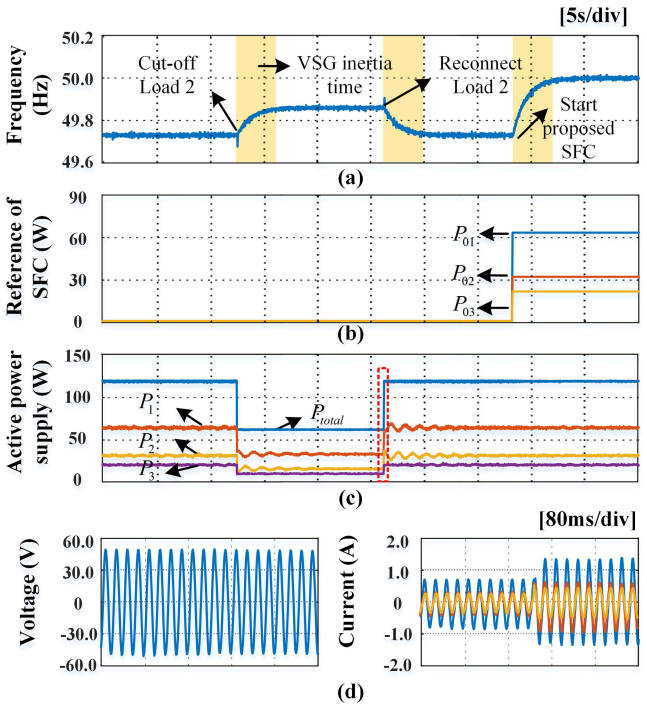

FIGURE 10. Primary control results. (a) Frequency waveforms of the VSG control. (b) Active power references of proposed SFC. (c) The supply and demand waveforms. (d) Voltage and current waveforms at load reconnection moment.

Fig. 10 shows the system performance after primary VSG control. Fig. 10(a) shows the frequency waveform of the primary VSG control. The settling time calculated according to (5) is 3.73s, which is drawn as the yellow zone in Fig. 5(a). The ROCOF is decreased significantly compared to the traditional droop control. The buffer time provided by the virtual inertia can be used in the proposed SFC. From (b) and (c) in Fig. 10, both practical power change and power reference change from SFC will influence the frequency. The power sharing among these DGs follows the proportion 6:3:2. (d) shows the voltage and current waveforms at the period of load 2 reconnection The period is pointed out in (c). The voltage is stabilized at 50V. The current changes according to the load change. The results in Fig. 10 verify that the VSG control runs well on the experimental testbed.

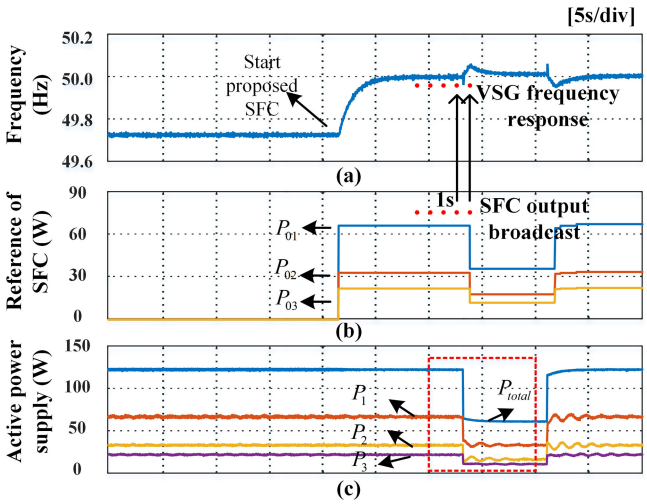

FIGURE 11. Proposed distributed event-trigger SFC results. (a) Frequency at PCC. (b) SFC broadcasts power references every 1s. (c) Active power supply and demand.

TABLE 4 Performance of Proposed SFC Iterations in 10 s

	DG 1	DG 2	DG 3
Communication triggers	1101	2098	1325

Fig. 11 shows the experiment results of the proposed distributed event-triggered SFC. The SFC broadcast period is 1s in Fig. 11. First, only primary control is operated. The frequency stabilizes at 49.72 Hz. Then the proposed SFC starts up to eliminate the frequency deviation and restore the frequency to 50 Hz. After the frequency achieves the steady state, load cut-off and reconnection are carried out. As shown in Fig. 11, at the end of 1s, the SFC broadcasts the power reference. The frequency starts to recover to 50 Hz. Even though there are power oscillations after load connection/disconnection, the proposed control can still generate proportional power reference values to guarantee stability.

The red brace in Fig. 11(c) marks a 10 s time slot which contains the moment of load disconnection. The iterations of the proposed control during 10 s are shown in Fig. 12. The sampling rate of the event-triggered algorithm is also chosen as 1ms. The event-triggered communication performance is listed in Table 4. The generated power reference values are satisfactory with more than 84% communication saved in 10 s.

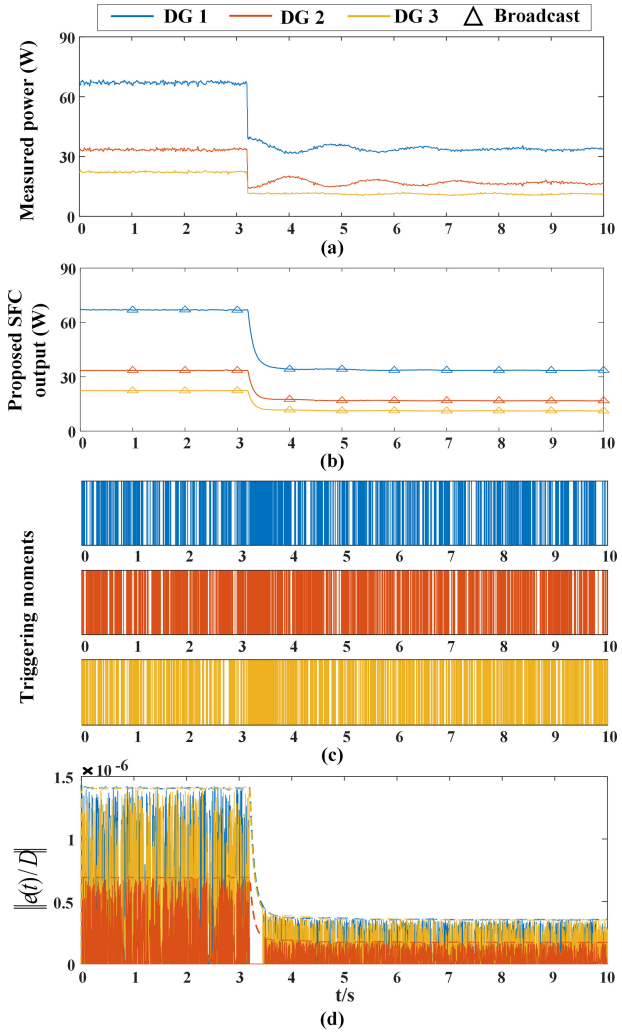

FIGURE 12. **Proposed SFC iterations in 10 s. (a) Measured active power of three DGs. (b) Iterations of control u with broadcast rate $T_s = 1$s. (c) Communication moments. (d) Estimate errors.**

The experiment results are similar to the simulation results in Section IV. The frequency convergence rate is accelerated with the proposed frequency restoration control method. The communication burden is highly reduced. Meanwhile, the generated power reference values maintain power sharing proportion accurately, unaffected by power oscillations. The practicability and effectiveness of the proposed event-triggered SFC are verified.

VI. CONCLUSION

In this paper, a novel distributed control for parallel inverters in an islanded microgrid is proposed. The proposed frequency restoration control accelerates the convergence rate of the frequency with virtual inertia. Meanwhile, the generated power reference values overcome the power oscillations and maintain the power sharing proportion. The communication burdens of the parallel inverter controllers are highly reduced under the proposed event-triggered conditions. The validation experiments are operated on the practical physical circuit, which verifies the practicability and effectiveness of the proposed control method.

REFERENCES

[1] J. Hu, Y. Shan, K. W. Cheng, and S. Islam, "Overview of power converter control in microgrids—Challenges, advances, and future trends," *IEEE Trans. Power Electron.*, vol. 37, no. 8, pp. 9907–9922, Aug. 2022.

[2] W. Xu, K. W. Chan, S. W. Or, S. L. Ho, and M. Liu, "A low-harmonic control method of bidirectional three-phase Z-source converters for vehicle-to-grid applications," *IEEE Trans. Transp. Electrific.*, vol. 6, no. 2, pp. 464–477, Jun. 2020.

[3] Y. Khayat et al., "On the secondary control architectures of AC microgrids: An overview," *IEEE Trans. Power Electron.*, vol. 35, no. 6, pp. 6482–6500, Jun. 2020.

[4] K. Feng, C. Liu, and Z. Song, "Hour-ahead energy trading management with demand forecasting in microgrid considering power flow constraints," *Energies*, vol. 12, no. 18, 2019, Art. no. 3494.

[5] R. M. Wright, "Understanding modern generator control," *IEEE Trans. Energy Convers.*, vol. 4, no. 3, pp. 453–458, Sep. 1989.

[6] Y. Deng, Y. Tao, G. Chen, G. Li, and X. He, "Enhanced power flow control for grid-connected droop-controlled inverters with improved stability," *IEEE Trans. Ind. Electron.*, vol. 64, no. 7, pp. 5919–5929, Jul. 2017.

[7] A. Lasheen, M. E. Ammar, H. H. Zeineldin, A. Al-Durra, M. F. Shaaban, and E. F. El-Saadany, "Assessing the impact of reactive power droop on inverter based microgrid stability," *IEEE Trans. Energy Convers.*, vol. 36, no. 3, pp. 2380–2392, Sep. 2021.

[8] M. A. Azghandi, S. M. Barakati, and A. Yazdani, "Passivity-based design of a fractional-order virtual capacitor for active damping of multiparalleled grid-connected current-source inverters," *IEEE Trans. Power Electron.*, vol. 37, no. 7, pp. 7809–7818, Jul. 2022.

[9] Q. C. Zhong and G. Weiss, "Synchronverters: Inverters that mimic synchronous generators," *IEEE Trans. Ind. Electron.*, vol. 58, no. 4, pp. 1259–1267, Apr. 2011.

[10] J. Liu, Y. Miura, H. Bevrani, and T. Ise, "Enhanced virtual synchronous generator control for parallel inverters in microgrids," *IEEE Trans. Smart Grid*, vol. 8, no. 5, pp. 2268–2277, Sep. 2017.

[11] Y. Hirase, K. Abe, K. Sugimoto, K. Sakimoto, H. Bevrani, and T. Ise, "A novel control approach for virtual synchronous generators to suppress frequency and voltage fluctuations in microgrids," *Appl. Energy*, vol. 210, pp. 699–710, 2018.

[12] H. Bevrani, B. François, and T. Ise, *Microgrid Dynamics and Control*. Hoboken, NJ, USA: Wiley, 2017.

[13] X. Meng, J. Liu, and Z. Liu, "A generalized droop control for grid-supporting inverter based on comparison between traditional droop control and virtual synchronous generator control," *IEEE Trans. Power Electron.*, vol. 34, no. 6, pp. 5416–5438, Jun. 2019.

[14] T. Wen, D. Zhu, X. Zou, B. Jiang, L. Peng, and Y. Kang, "Power coupling mechanism analysis and improved decoupling control for virtual synchronous generator," *IEEE Trans. Power Electron.*, vol. 36, no. 3, pp. 3028–3041, Mar. 2021.

[15] L. Zhou et al., "Harmonic current and inrush fault current coordinated suppression method for VSG under non-ideal grid condition," *IEEE Trans. Power Electron.*, vol. 36, no. 1, pp. 1030–1042, Jan. 2021.

[16] Y. Guan, J. C. Vasquez, and J. M. Guerrero, "Coordinated secondary control for balanced discharge rate of energy storage system in islanded AC microgrids," *IEEE Trans. Ind. Appl.*, vol. 52, no. 6, pp. 5019–5028, Non./Dec. 2016.

[17] Y. Khayat et al., "Decentralized frequency control of AC microgrids: An estimation-based consensus approach," *IEEE J. Emerg. Sel. Topics Power Electron.*, vol. 9, no. 5, pp. 5183–5191, Oct. 2021.

[18] B. Liu, T. Wu, Z. Liu, and J. Liu, "A small-ac-signal injection-based decentralized secondary frequency control for droop-controlled islanded microgrids," *IEEE Trans. Power Electron.*, vol. 35, no. 11, pp. 11634–11651, Nov. 2020.

[19] S. Deng, L. Chen, X. Lu, T. Zheng, and S. Mei, "Distributed finite-time secondary frequency control of islanded microgrids with enhanced operational flexibility," *IEEE Trans. Energy Convers.*, vol. 36, no. 3, pp. 1733–1742, Sep. 2021.

[20] N. Sarrafan, M.-A. Rostami, J. Zarei, R. Razavi-Far, M. Saif, and T. Dragičević, "Improved distributed prescribed finite-time secondary control of inverter-based microgrids: Design and real-time implementation," *IEEE Trans. Ind. Electron.*, vol. 68, no. 11, pp. 11135–11145, Nov. 2021.
[21] D. Zhao, C. Zhang, Y. Sun, S. Li, B. Sun, and Y. Li, "Distributed robust frequency restoration and active power sharing for autonomous microgrids with event-triggered strategy," *IEEE Trans. Smart Grid*, vol. 12, no. 5, pp. 3819–3834, Sep. 2021.
[22] L. Ding, Q.-L. Han, and X.-M. Zhang, "Distributed secondary control for active power sharing and frequency regulation in islanded microgrids using an event-triggered communication mechanism," *IEEE Trans. Ind. Informat.*, vol. 15, no. 7, pp. 3910–3922, Jul. 2019.
[23] Y. Wang, T. L. Nguyen, Y. Xu, Z. Li, Q.-T. Tran, and R. Caire, "Cyber-physical design and implementation of distributed event-triggered secondary control in islanded microgrids," *IEEE Trans. Ind. Appl.*, vol. 55, no. 6, pp. 5631–5642, Nov./Dec. 2019.
[24] W. Hu, Z. Wu, X. Lv, and V. Dinavahi, "Robust secondary frequency control for virtual synchronous machine-based microgrid cluster using equivalent modeling," *IEEE Trans. Smart Grid*, vol. 12, no. 4, pp. 2879–2889, Jul. 2021.
[25] L. Subramanian, V. Debusschere, H. B. Gooi, and N. Hadjsaid, "A cooperative rate-based model predictive framework for flexibility management of DERs," *IEEE Trans. Energy Convers.*, vol. 36, no. 4, pp. 2724–2733, Dec. 2021.
[26] S. Trip and C. De Persis, "Distributed optimal load frequency control with non-passive dynamics," *IEEE Trans. Control Netw. Syst.*, vol. 5, no. 3, pp. 1232–1244, Sep. 2018.
[27] E. A. Coddington and N. Levinson, *Theory of Ordinary Differential Equations*. New York, NY, USA: Tata McGraw-Hill Education, 1955.
[28] F. Dörfler and S. Grammatico, "Gather-and-broadcast frequency control in power systems," *Automatica*, vol. 79, pp. 296–305, 2017.
[29] W. Ren and Y. Cao, *Distributed Coordination of Multi-Agent Networks: Emergent Problems, Models, and Issues*. Berlin, Germany: Springer, 2011.
[30] J. P. La Salle, *The Stability of Dynamical Systems*. Philadelphia, PA, USA: SIAM, 1976.
[31] P. Tabuada, "Event-triggered real-time scheduling of stabilizing control tasks," *IEEE Trans. Autom. Control*, vol. 52, no. 9, pp. 1680–1685, Sep. 2007.
[32] Y. Chen, C. Li, D. Qi, Z. Li, Z. Wang, and J. Zhang, "Distributed event-triggered secondary control for islanded microgrids with proper trigger condition checking period," *IEEE Trans. Smart Grid*, vol. 13, no. 2, pp. 837–848, Mar. 2022.
[33] Y.-D. Wu, M.-F. Ge, Z.-W. Liu, W.-Y. Zhang, and W. Wei, "Distributed CPS-based secondary control of microgrids with optimal power allocation and limited communication," *IEEE Trans. Smart Grid*, vol. 13, no. 1, pp. 82–95, Jan. 2022.
[34] M. Chen, X. Xiao, and J. M. Guerrero, "Secondary restoration control of islanded microgrids with a decentralized event-triggered strategy," *IEEE Trans. Ind. Informat.*, vol. 14, no. 9, pp. 3870–3880, Sep. 2018.

KUO FENG received the B.Eng. and M.Eng. degrees in electrical engineering and automation from Wuhan University, Wuhan, China, in 2015 and 2018, respectively. She is currently working toward the Ph.D. degree in electrical and electronic engineering from the City University of Hong Kong, Hong Kong. Her research interests include frequency and voltage regulation, economic dispatch, distributed control, optimization, and virtual power technologies for microgrids.

CHUNHUA LIU (Senior Member, IEEE) received the B.Eng. and M.Eng. degrees in automatic control from the Beijing Institute of Technology, Beijing, China, and the Ph.D. degree in electrical and electronic engineering, The University of Hong Kong, Hong Kong, in 2002, 2005, and 2009, respectively. He is currently an Associate Professor in electrical and electronic engineering with the School of Energy and Environment, City University of Hong Kong, Hong Kong. He has authored or coauthored more than 250 refereed papers in his research areas, which include electric machines and drives, electric vehicles and aircrafts, electric robotics and ships, renewables and microgrids, power electronics, and wireless power transfer. In addition, he is a RGC Research Fellow, Distinguish Lecturer of IEEE Vehicular Technology Society, and World's Top 2% Scientists according to metrics compiled by Stanford University. Dr. Liu is an Associate Editor for IEEE TRANSACTIONS ON INDUSTRIAL ELECTRONICS, the Editor of IEEE TRANSACTIONS ON VEHICULAR TECHNOLOGY, IEEE TRANSACTIONS ON ENERGY CONVERSION, and IEEE POWER ENGINEERING LETTERS. He is also the Editor of *Energies*, the Subject Editor of *IET – Renewable Power Generation*, an Associate Editor for the *Open Journal of the Industrial Electronics Society*, IEEE CHINESE JOURNAL OF ELECTRICAL ENGINEERING, *CES Transactions on Electrical Machines and Systems*, and *Elsevier Green Energy and Intelligent Transportation*, and the Editor of IEEE Transactions on Magnetics – Conference. In addition, he is the Chair and Founder of Hong Kong Chapter, IEEE Vehicular Technology Society, and Hong Kong and Guangzhou Joint Chapter, IEEE Industrial Electronics Society.